

An Experimental Study of the Laminar Flow Separation on a Low-Reynolds-Number Airfoil

An experimental study was conducted to characterize the transient behavior of laminar flow separation on a NASA low-speed GA (W)-1 airfoil at the chord Reynolds number of 70,000. In addition to measuring the surface pressure distribution around the airfoil, a high-resolution particle image velocimetry (PIV) system was used to make detailed flow field measurements to quantify the evolution of unsteady flow structures around the airfoil at various angles of attack (AOAs). The surface pressure and PIV measurements clearly revealed that the laminar boundary layer would separate from the airfoil surface, as the adverse pressure gradient over the airfoil upper surface became severe at $AOA \geq 8.0$ deg. The separated laminar boundary layer was found to rapidly transit to turbulence by generating unsteady Kelvin–Helmholtz vortex structures. After turbulence transition, the separated boundary layer was found to reattach to the airfoil surface as a turbulent boundary layer when the adverse pressure gradient was adequate at $AOA < 12.0$ deg, resulting in the formation of a laminar separation bubble on the airfoil. The turbulence transition process of the separated laminar boundary layer was found to be accompanied by a significant increase of Reynolds stress in the flow field. The reattached turbulent boundary layer was much more energetic, thus more capable of advancing against an adverse pressure gradient without flow separation, compared to the laminar boundary layer upstream of the laminar separation bubble. The laminar separation bubble formed on the airfoil upper surface was found to move upstream, approaching the airfoil leading edge as the AOA increased. While the total length of the laminar separation bubble was found to be almost unchanged ($\sim 20\%$ of the airfoil chord length), the laminar portion of the separation bubble was found to be slightly stretched, and the turbulent portion became slightly shorter with the increasing AOA. After the formation of the separation bubble on the airfoil, the increase rate of the airfoil lift coefficient was found to considerably degrade, and the airfoil drag coefficient increased much faster with increasing AOA. The separation bubble was found to burst suddenly, causing airfoil stall, when the adverse pressure gradient became too significant at $AOA > 12.0$ deg.

[DOI: 10.1115/1.2907416]

Hui Hu
Assistant Professor
e-mail: huhui@iastate.edu

Zifeng Yang
Graduate Student

Department of Aerospace Engineering,
Iowa State University,
Ames, IA 50011

1 Introduction

Low-Reynolds-number airfoil aerodynamics is important for both military and civilian applications. These applications include propellers, sailplanes, ultralight man-carrying/man-powered aircraft, high-altitude vehicles, wind turbines, unmanned aerial vehicles (UAVs), and microAir vehicles (MAVs). Nondimensional chord Reynolds number (Re_C) is defined as the cruise speed multiplied by the mean wing chord and divided by the kinematic viscosity of air. For the applications listed above, the combination of small length scale and low flight velocities results in flight regimes with low wing-chord Reynolds number (i.e., chord Reynolds numbers, Re_C , ranging from 10,000 to 500,000). The aerodynamic design methods and principles developed over the past 40 years have produced efficient airfoils for conventional, large-scale, high-speed aircraft whose chord Reynolds numbers are usually in the range of 10^6 – 10^9 . It is well known that the aerodynamic performance of airfoils that are optimal for conventional, large-scale and high-speed aircraft (therefore, high chord Reynolds number) significantly degrades when used for low-Reynolds-number applications where the chord Reynolds numbers are several orders smaller. While conventional airfoil design principles usually either neglect viscous effects or restrict its influence

to a very thin region near the airfoil surface at high Reynolds numbers, the predominance of viscous effects in low-Reynolds-number applications would result in boundary layers rapidly growing and easily separating from the surfaces of airfoils.

It is well known that the boundary layers on low-Reynolds-number airfoils remain laminar at the onset of the pressure recovery unless artificially tripped. The behavior of the laminar boundary layers on low-Reynolds-number airfoils significantly affects the aerodynamic performances of the airfoils. Since laminar boundary layers are unable to withstand any significant adverse pressure gradient, laminar flow separation is usually found on low-Reynolds-number airfoils. Postseparation behavior of laminar boundary layers accounts for the deterioration in the aerodynamic performances of low-Reynolds-number airfoils. The deterioration is exhibited by an increase in drag and decrease in lift. Extensive reviews about aerodynamics of low-Reynolds-number airfoils and the dependence of the laminar flow separation phenomena on the chord Reynolds numbers can be found at Tani [1], Carmichael [2], Lissaman [3], Mueller [4] and Gad-el-Hak [5]. It has been suggested that the separated laminar boundary layers would rapidly transit to turbulence, and then reattach to the airfoil surface as a turbulent boundary layer when the adverse pressure gradient over the airfoil surface is adequate [6]. This would result in the formation of a laminar separation bubble, as schematically shown in Fig. 1. As the adverse pressure gradient becomes more severe with the increasing angle of attack, the separation bubble would suddenly burst, which will subsequently result in airfoil stall.

A good physical understanding is essential in order to control

Contributed by the Fluids Engineering Division of ASME for publication in the JOURNAL OF FLUIDS ENGINEERING. Manuscript received April 7, 2007; final manuscript received January 31, 2008; published online April 25, 2008. Assoc. Editor: Hamid Johari.

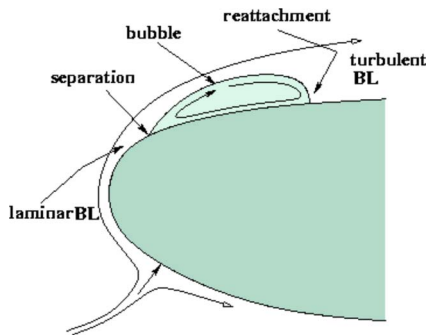


Fig. 1 Schematic of a laminar separation bubble formed on a low-Reynolds-number airfoil

the laminar flow separations and suppress the burst of the laminar separation bubbles for better aerodynamic performances of low-Reynolds-number airfoils. This requires a detailed knowledge about transient behavior of the separated laminar boundary layers and the evolution of laminar separation bubbles. Although extensive experimental studies have been conducted to investigate laminar flow separation, transition, and reattachment on low-Reynolds-number airfoils, the majority of those previous studies were carried out by using pointwise flow diagnostic techniques, such as hot-wire anemometry [7–10], hot-film anemometry [11,12] and laser Doppler velocimetry [13–15] to conduct flow velocity measurements at limited points of interest. A common shortcoming of such pointwise flow measurements is the incapability of providing spatial correlation of the unsteady flow structures to effectively reveal the transient behavior of the laminar flow separation. The availability of temporally synchronized and spatially resolved flow field measurements is highly desirable in order to elucidate underlying physics to improve our understanding about the laminar boundary layer separation, transition, and reattachment processes on low-Reynolds-number airfoils. Advanced flow diagnostic techniques, such as particle image velocimetry (PIV), are capable of providing such information.

Surprisingly, only very few experimental studies were recently conducted to provide temporally synchronized and spatially resolved flow field measurements to quantify the transient behavior of the laminar boundary layers on low-Reynolds-number airfoils [16–19]. Very little in the literature can be found to correlate detailed flow field measurements with the airfoil surface pressure measurements to investigate laminar flow separation, transition, and reattachment as well as the evolution of laminar separation bubbles on low-Reynolds-number airfoils. In this study, we conducted a detailed experimental study to characterize the transient behavior of laminar flow separation, transition, and reattachment on a low-Reynolds-number airfoil at $Re_c=70,000$. In addition to mapping the surface pressure distribution around the airfoil with pressure sensors, a high-resolution PIV system was used to make detailed flow field measurements to quantify the occurrence and behavior of laminar boundary layer separation, transition, and reattachment on the low-Reynolds-number airfoil. The detailed flow field measurements were correlated with the surface pressure measurements to elucidate the underlying physics associated with the separation, transition, and reattachment processes of the laminar boundary layer. To the best knowledge of the authors, this is the first effort of its nature. The primary objective of the present study is to gain further insight into the fundamental physics of laminar flow separation, transition, and reattachment as well as the evolution of laminar separation bubble formed on low-Reynolds-number airfoils. In addition, the quantitative surface pressure and flow field measurements will be used as the database for the validation of computational fluid dynamics (CFD) simulations of such complex flow phenomena for the optimum design of low-Reynolds-number airfoils [20].

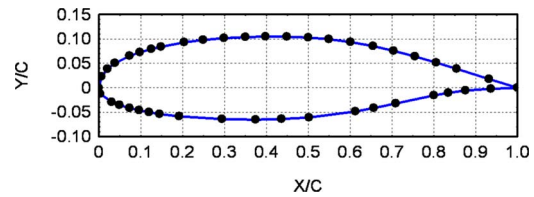


Fig. 2 GA(W)-1 airfoil geometry and pressure tap locations

2 Experimental Setup and the Studied Airfoil

The experiments were performed in a closed-circuit low-speed wind tunnel located in the Aerospace Engineering Department of Iowa State University. The tunnel has a test section with a $1.0 \times 1.0 \text{ ft}^2$ ($30 \times 30 \text{ cm}^2$) cross section and optically transparent walls. The tunnel has a contraction section upstream of the test section with honeycomb, screen structures, and cooling system installed ahead of the contraction section to provide uniform low turbulent incoming flow to enter the test section.

Figure 2 shows the schematic of the airfoil used in the present study: a GA (W)-1 airfoil (also labeled as NASA LS(1)-0417). The GA (W)-1 has a maximum thickness of 17% of the chord length. Compared to standard NACA airfoils, the GA (W)-1 airfoil was especially designed for low-speed general aviation applications with a large leading-edge radius in order to flatten the peak in pressure coefficient near the airfoil nose to discourage flow separation [21]. The chord length of the airfoil model is 101 mm, i.e., $C=101 \text{ mm}$, for the present study. The flow velocity at the inlet of the test section was set as $U_\infty=10.7 \text{ m/s}$, which corresponds to a chord Reynolds number of $Re_c \approx 70,000$.

The airfoil model is equipped with 43 pressure taps at its median span with the spanwise length of the airfoil being 1.0 ft. The locations of the pressure taps are indicated in Fig. 2. The 43 pressure taps were connected by plastic tubing to 43 channels of a pressure acquisition system (Model DSA3217, Scanivalve Corp). The DSA3217 digital sensor arrays incorporate temperature compensated piezoresistive pressure sensors with a pneumatic calibration valve, RAM, 16 bit A/D converter, and a microprocessor in a compact self-contained module. The precision of the pressure acquisition system is $\pm 0.2\%$ of the full scale ($\pm 10 \text{ in. H}_2\text{O}$). During the experiment, each pressure transducer input was scanned at 400 Hz for 20 s. The pressure coefficient distributions, $C_p=(P - P_\infty)/(\frac{1}{2}\rho U_\infty^2)$, around the airfoil at various angles of attack were measured by using the pressure acquisition system. The lift and drag coefficients ($C_l=l/(\frac{1}{2}\rho U_\infty^2 C)$ and $C_d=d/(\frac{1}{2}\rho U_\infty^2 C)$) of the 2D airfoil were determined by numerically integrating the pressure distribution around the airfoil.

Figure 3 shows the schematic of the experimental setup used for the PIV measurement. The test airfoil was installed in the middle of the test section. A PIV system was used to make flow velocity field measurements along the chord at the middle span of the airfoil. The flow was seeded with $\sim 1 \mu\text{m}$ oil droplets. Illumination was provided by a double-pulsed Nd:YAG (yttrium aluminum garnet) laser (NewWave Gemini 200) adjusted on the second harmonic and emitting two laser pulses of 200 mJ at a wavelength of 532 nm with a repetition rate of 10 Hz. The laser beam was shaped into a sheet by a set of mirrors, spherical and cylindrical lenses. The thickness of the laser sheet in the measurement region is about 0.5 mm. A high-resolution 12 bit (1376×1040 pixels) charge-coupled device (CCD) camera was used for PIV image acquisition with the axis of the camera perpendicular to the laser sheet. The CCD camera and the double-pulsed Nd:YAG lasers were connected to a workstation (host computer) via a Digital Delay Generator (Berkeley Nucleonics, Model 565), which controlled the timing of the laser illumination and the image acquisition. In the present study, a careful pretest, which includes testing different seeding methods, applying different paints to the airfoil

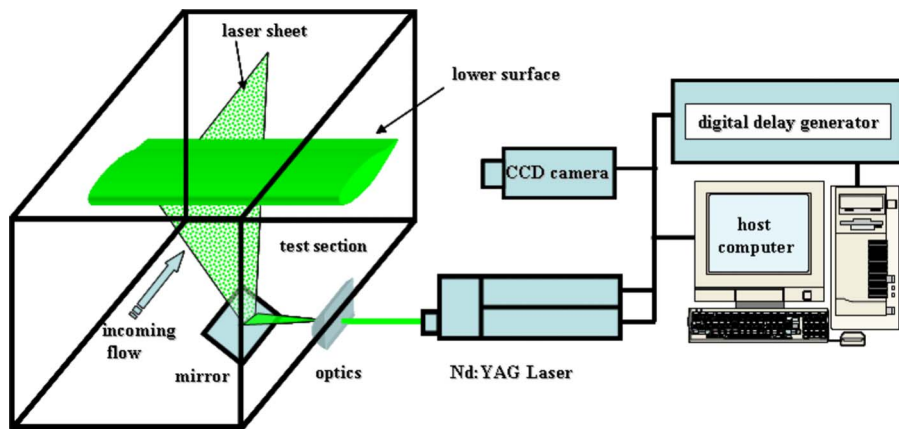


Fig. 3 Schematic of the experimental setup for the PIV measurements

model as well as adjusting laser excitation energy level, camera positions, and optic lens arrangements, was conducted in order to minimize the reflection from the airfoil surface for the near wall PIV measurements.

Instantaneous PIV velocity vectors were obtained by a frame to frame cross-correlation technique involving successive frames of patterns of particle images in an interrogation window of 32×32 pixels. An effective overlap of 50% was employed for PIV image processing. After the instantaneous velocity vectors ($\mathbf{u}_i, \mathbf{v}_i$) were determined, the spanwise vorticity (ω_z) could be derived. The time-averaged quantities such as mean velocity (U, V), turbulent velocity fluctuations ($\overline{u'}, \overline{v'}$), normalized Reynolds stress ($\overline{\tau} = -\overline{u'v'}/U_\infty^2$), and normalized turbulent kinetic energy (TKE $= 0.5 * (\overline{u'^2} + \overline{v'^2})/U_\infty^2$) were obtained from a cinema sequence of 400 frames of instantaneous velocity fields. The measurement uncertainty level for the velocity vectors is estimated to be within 2% and 5% for the turbulent velocity fluctuations ($\overline{u'}, \overline{v'}$), Reynolds stress, and turbulent kinetic energy calculations. The uncertainty level of the spanwise vorticity data is expected to be within 10.0%. It should be noted that the surface pressure mapping and PIV measurements are designed to acquire statistical data instead of time-resolved measurements due to the limited sampling rates of the surface pressure mapping and PIV measurements.

3 Experimental Results and Discussions

3.1 Measured Surface Pressure Distribution Around the Airfoil. Figure 4 shows the measured surface pressure coefficient distributions around the GA (W)-1 airfoil as the angle of attack changes from 6.0 deg to 14.0 deg. While the surface pressure distribution on the lower surface of the airfoil does not notably

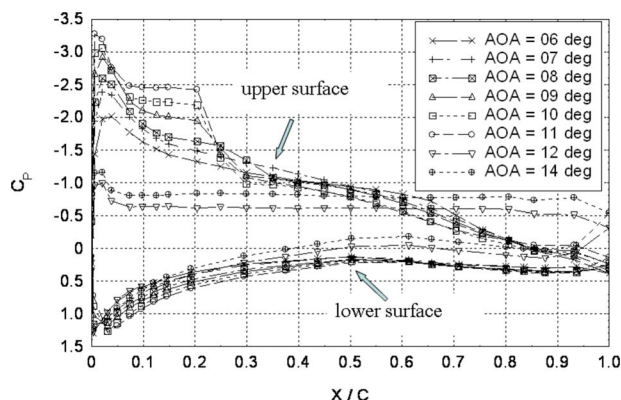


Fig. 4 Surface pressure distribution profiles around the airfoil

change with the increasing angle of attack (up to 12.0 deg), the surface pressure distribution on the upper surface of the airfoil was found to significantly vary at different angles of attack. As the angle of attack (AOA) was relatively small (i.e., $AOA < 8.0$ deg), the surface pressure coefficient profiles along the airfoil upper surface were found to rapidly reach their negative peaks at locations quite near to the airfoil leading edge, then the surface pressure gradually and smoothly recovered over the upper surface of the airfoil up to the airfoil trailing edge. As the AOA increases to $8.0 \leq AOA < 12.0$ deg, a distinctive characteristic of the surface pressure coefficient profiles is the existence of a region of nearly constant pressure (i.e., pressure plateau region) at $X/C \approx 0.05-0.25$. Sudden increase in surface pressure coefficient was found following the pressure plateau region. Further downstream, the surface pressure was found to gradually and smoothly recover, which is similar as those cases with relatively low AOAs. Such a characteristic of the surface pressure profiles is actually closely related to laminar flow separation and the formation of laminar separation bubbles on low-Reynolds-number airfoils.

As schematically illustrated in Fig. 5, Russell [22] suggested a theoretic model to characterize the laminar separation bubbles formed on low-Reynolds-number airfoils. Based on the theoretic model of Russell [22], the critic points (the separation, transition, and reattachment points) of a laminar separation bubble formed on a low-Reynolds-number airfoil can be determined from the surface pressure measurements. The separation point refers to the location from where the laminar boundary layer separates from the airfoil surface. The transition point refers to the onsite point at where the separated laminar boundary layer begins to transit to turbulence. The reattachment point refers to the location where the separated boundary layer reattaches to the airfoil surface after transition. As suggested by Russell [22], a laminar separation bubble formed on a low-Reynolds-number airfoil includes two portions: a laminar portion and a turbulent portion. The location of the pressure plateau is coincident with that of the laminar portion of the separation bubble. The starting point of the pressure plateau indicates the location where the laminar boundary layer separates from the airfoil surface (i.e., the separation point). Since the transition of the separated laminar boundary layer to turbulence will result in a rapid pressure rise brought about by fluid entrainment, the termination of the pressure plateau can be used to locate the transition point, at where the transition of the separated laminar boundary layer to turbulence begins to occur. The pressure rise due to the turbulence transition often overshoots the inviscid pressure that exists at the reattachment location. Therefore, the location of the point of equality between the actual and inviscid surface pressure marks the location of reattachment (i.e., the reattachment point).

Following the work of Russell [22], the locations of the critic

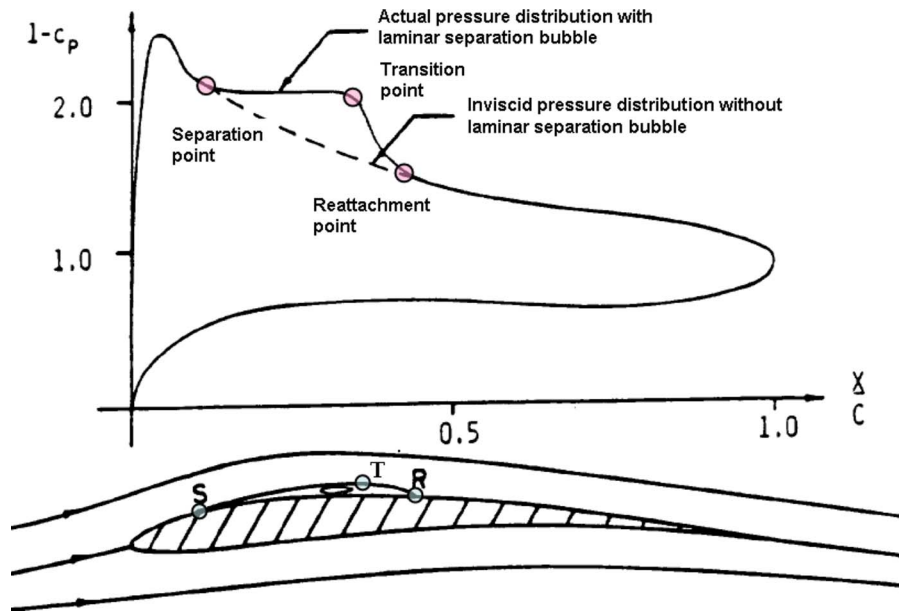


Fig. 5 Pressure distribution on an airfoil with laminar separation bubble (Russell [22])

points (the separation, transition, and reattachment points) of laminar separation bubbles at different AOA were estimated based on the measured airfoil surface pressure profiles given in Fig. 4. A summation of the locations of separation, transition, and reattachment points on the GA(W)-1 airfoil at different AOA is given in Fig. 6. The uncertainties of the estimated locations of the critical points is about 2.0% of chord length due to the limited numbers of the pressure taps available in the region, which are shown in the figure as the error bars. As the AOA increases, the laminar separation bubble was found to move upstream to approach the airfoil leading edge. The total length of the separation bubble (i.e., the distance between the separation and reattachment points), which is about 20% of the chord length, was found to be almost unchanged regardless of the angles of attack. Following the terminology used by Horton [6], the length of the laminar portion of the separation bubble is defined as the distance between the separation point and the transition point, and the turbulent portion length corresponds to the distance between the transition

point and the reattachment point. From the experimental results given in Fig. 6, it can be seen that, while the length of the laminar portion of the separation bubble was found to slightly increase as the AOA increases, the turbulent portion became slightly shorter with the increasing AOA.

As the AOA became greater than 12.0 deg, the magnitude of the negative pressure coefficient peak near the airfoil leading edge was found to significantly decrease. As shown in Fig. 4, the surface pressure over most of the airfoil upper surface was found to be nearly constant. Such a surface pressure distribution indicates that airfoil is in stalled state [23–25], which is confirmed from the PIV measurements given in Fig 7.

3.2 PIV Measurement Results. While the surface pressure measurements can be used to quantify the global characteristics of the laminar separation bubble formed on the low-Reynolds-number airfoil, quantitative flow field measurements taken by using a high-resolution PIV system can reveal much more details

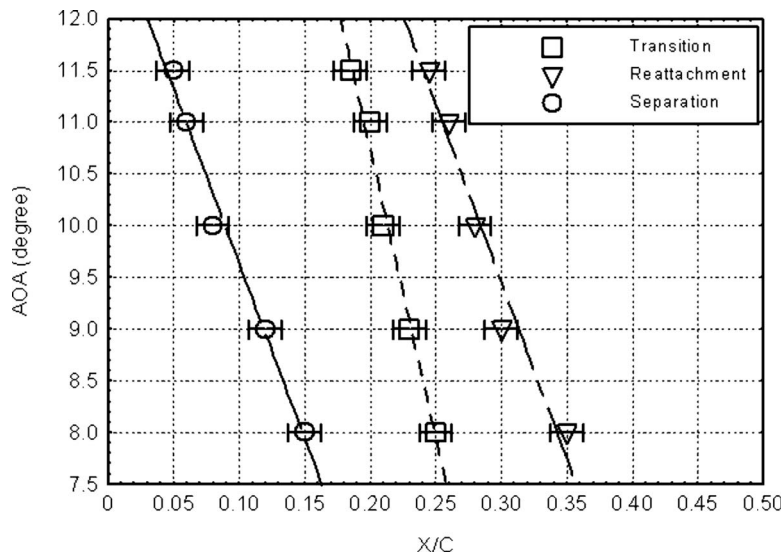
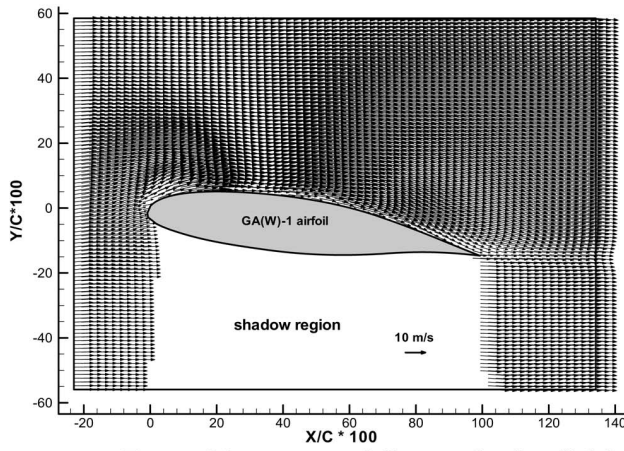
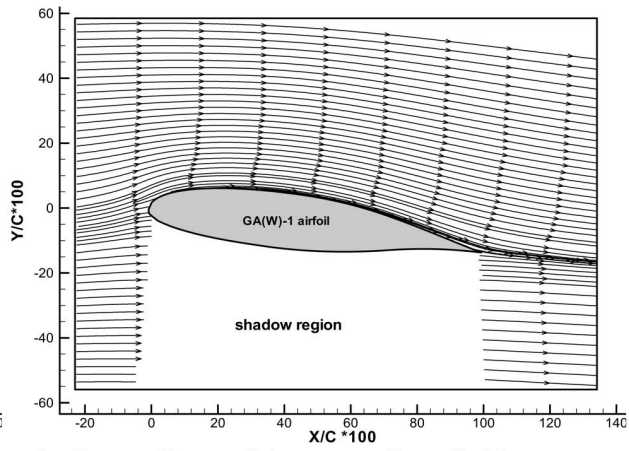


Fig. 6 The estimated locations of the separation points, transition points, and reattachment points at various AOA

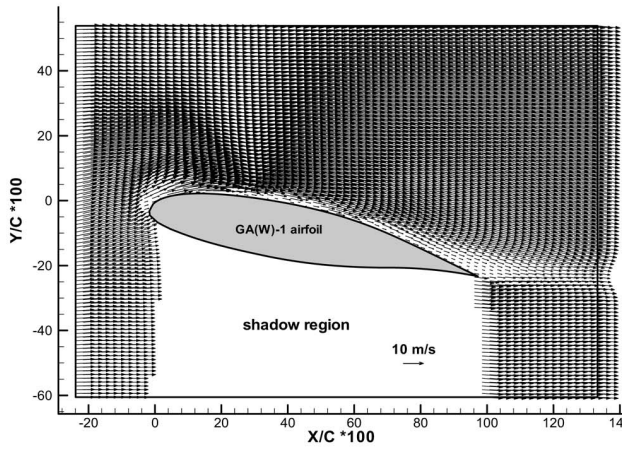


a. Ensemble-averaged flow velocity field

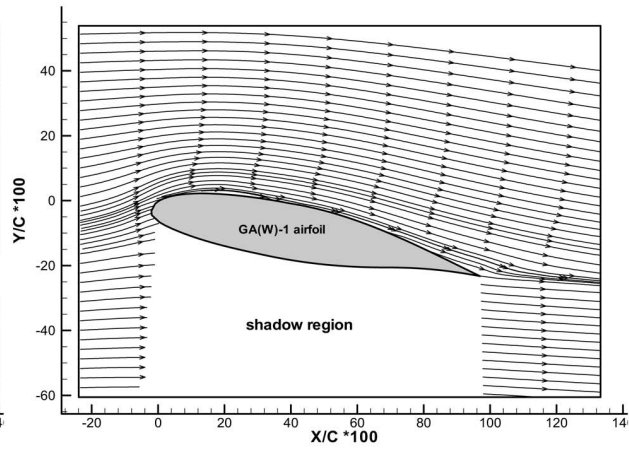


b. Streamlines of the mean flow field

A. AOA = 6.0 degrees

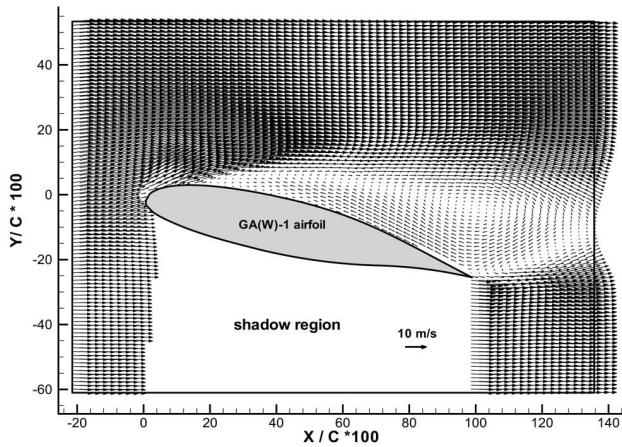


a. Ensemble-averaged flow velocity field

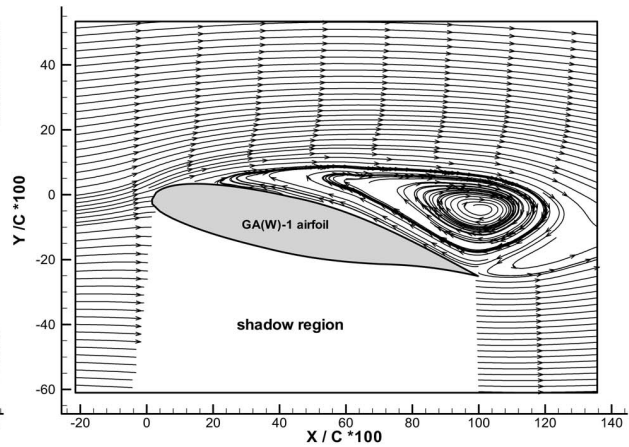


b. Streamlines of the mean flow field

B. AOA = 10.0 degrees



a. Ensemble-averaged flow velocity field



b. Streamlines of the mean flow field

C. AOA = 12.0 degrees

Fig. 7 PIV measurement results at various AOAs

about the transient behavior of laminar flow separation and the evolution of a laminar separation bubble formed on the airfoil. In the present study, PIV measurements were conducted at three spatial resolution levels: a coarse level to visualize the global features of the flow structures around the airfoil at various AOAs with the measurement window size being about $160 \times 120 \text{ mm}^2$, a refined

level to reveal the transient behavior of the laminar flow separation process near the nose of the airfoil with a measurement window size of about $40 \times 20 \text{ mm}^2$, and a superfine level to elucidate the details about the turbulence transition and the reattachment of the separated boundary layer to the airfoil surface at the rear portion of the separation bubble with a measurement window size of

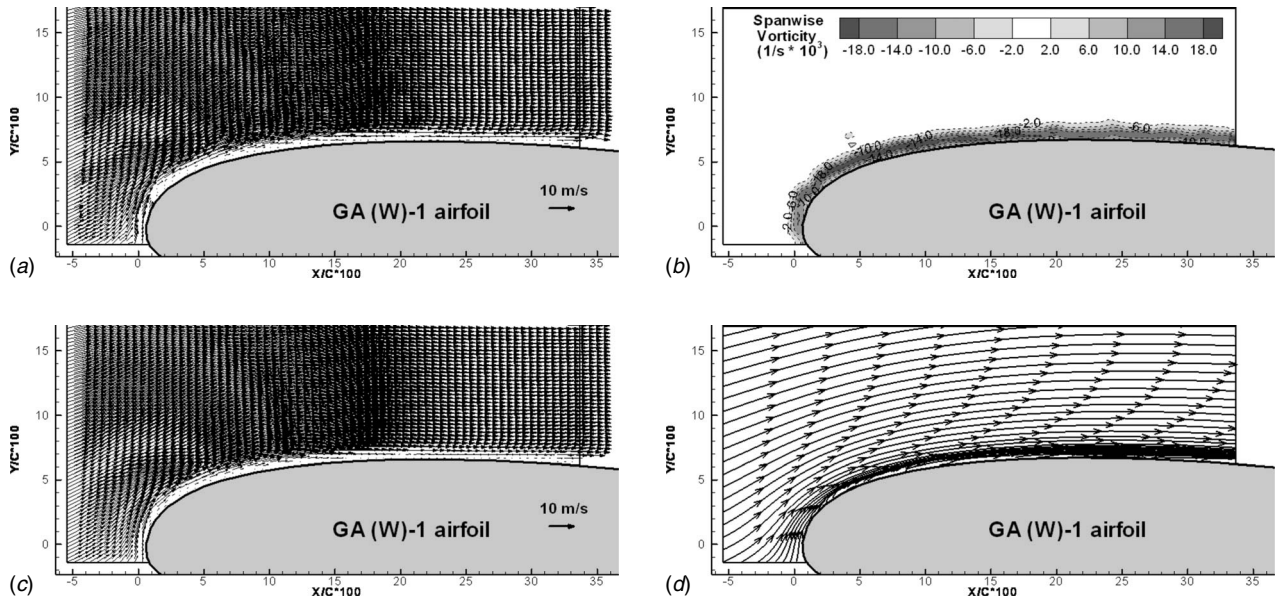


Fig. 8 PIV measurements near the airfoil leading edge with AOA=6.0 deg; (a) instantaneous velocity vectors; (b) instantaneous vorticity distribution; (c) ensemble-averaged velocity vectors; and (d) streamlines of the mean flow

about $16 \times 10 \text{ mm}^2$. The time interval between the double pulsed laser illumination for the PIV measurements was set as $\Delta t = 40.0 \mu\text{s}$, $14.0 \mu\text{s}$, and $4.0 \mu\text{s}$, respectively. The effective resolutions of the PIV measurements (i.e., grid sizes) were $\Delta/C = 0.018$, 0.0045 , and 0.0018 , respectively.

Figure 7 shows the PIV measurement results at the coarse resolution level. As clearly revealed by the ensemble-averaged velocity distribution and the streamlines of the mean flow around the airfoil, incoming flow streams faithfully follow the streamlined profile of the airfoil when the AOA is relatively small (i.e., AOA < 8.0 deg). No flow separation was found on the airfoil upper surface when the adverse pressure gradient is rather mild at relatively small AOA. Since the flow streams can firmly attach to the airfoil surface, they smoothly leave the airfoil at the trailing edge, which results in a very small wake region (i.e., the region

with velocity deficits) downstream of the airfoil. The small wake region downstream of the airfoil indicates a small aerodynamic drag force acting on the airfoil, which is confirmed from the drag coefficient measurement results given in Fig. 12.

As the AOA increases to 8.0–11.0 deg, the surface pressure measurement results given in Fig. 4 indicate that a laminar separation bubble would be generated on the upper surface of the airfoil. However, since the height of the separation bubble is very small (only $\sim 1.0\%$ of the chord length based on the refined PIV measurement results shown in Figs. 9 and Fig. 10), the laminar separation bubble cannot be clearly revealed from the PIV measurement results shown in Fig. 7(B) due to the limited spatial resolution of the PIV measurements (i.e., $\Delta/C \approx 0.018$). It has been suggested that the separated laminar boundary layer would firmly reattach to the airfoil upper surface at the downstream of

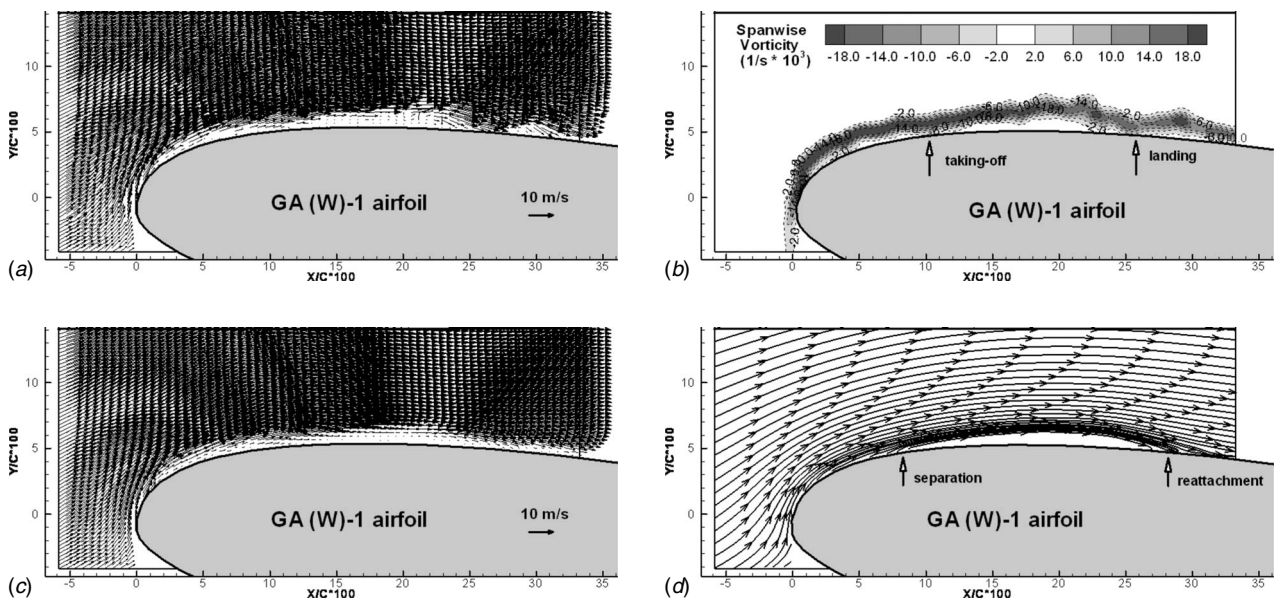


Fig. 9 PIV measurements near the airfoil leading edge with AOA=10.0 deg; (a) instantaneous velocity vectors; (b) instantaneous vorticity distribution; (c) ensemble-averaged velocity vectors; and (d) streamlines of the mean flow

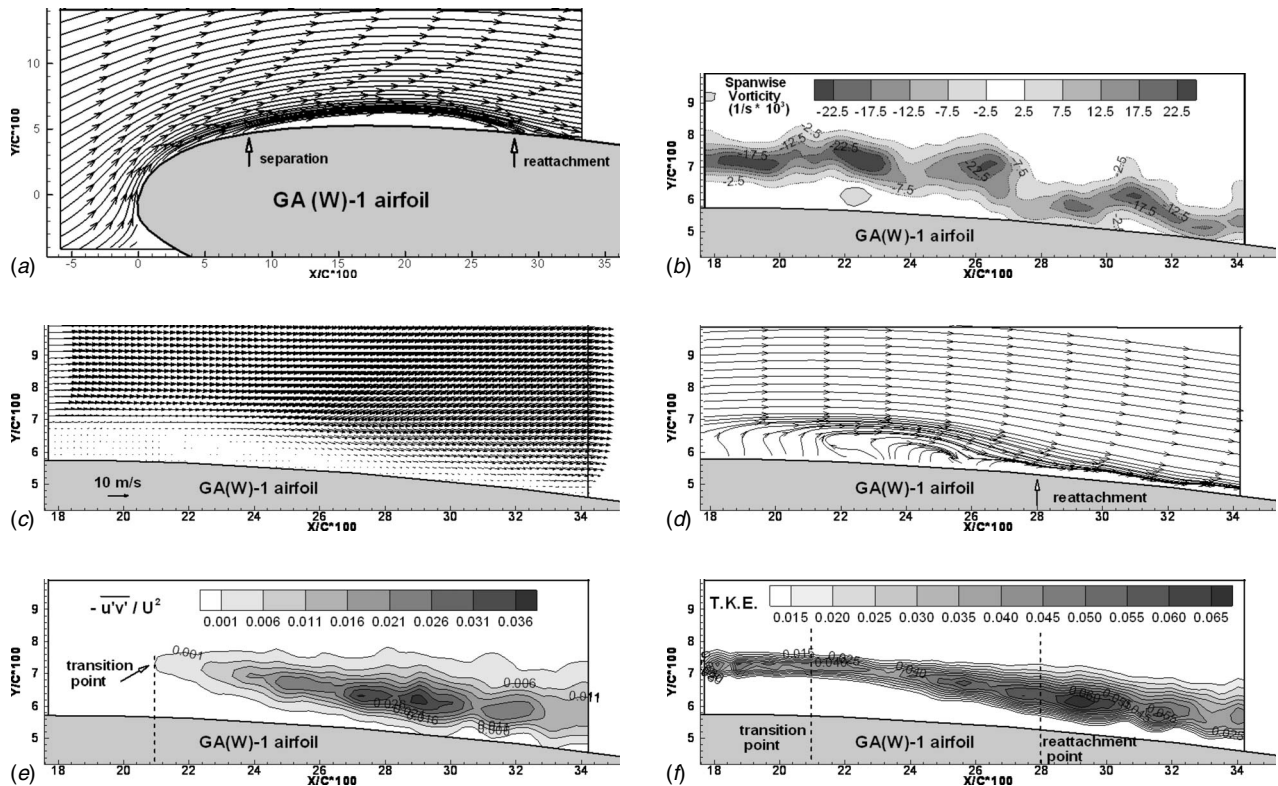


Fig. 10 PIV measurement results at the rear portion of the separation bubble with AOA=10.0 deg; (a) instantaneous velocity field; (b) instantaneous vorticity distribution; (c) ensemble-averaged velocity field; (d) streamlines of the mean flow; (e) normalized Reynolds stress distribution; and (f) normalized turbulent kinetic energy distribution

the reattachment point all the way to the airfoil trailing edge [6,22,23]. The mean velocity vectors and streamlines of the mean flow shown in Fig. 7(B) reveal that incoming flow streams smoothly leave the airfoil at the trailing edge at AOA=10.0 deg, which confirms the reattachment of the separated boundary layer to the airfoil upper surface downstream of the laminar separation bubble. As a result of the reattachment of the separated boundary layer, the wake region downstream of the airfoil was found to be reasonably small even though a separated bubble was already formed on the airfoil upper surface. Compared to those cases at smaller AOA (such as the case shown in Figs. 7(A) with AOA =6.0 deg), the size of the wake region for the cases with the separation bubbles generated on the airfoil upper surface becomes slightly larger, indicating a slightly increased aerodynamic drag force acting on the airfoil, which is confirmed from the airfoil drag coefficient measurement results given in Fig. 12.

The adverse pressure gradient over the upper surface of the airfoil becomes more and more severe as the AOA increases. The surface pressure measurement results given in Fig. 4 indicate that the separation bubble would burst, eventually causing airfoil stall when the AOA becomes greater than 12.0 deg. The large-scale flow separation over almost the entire upper surface of the airfoil due to the burst of the laminar separation bubble is visualized clearly and quantitatively from the PIV measurement results given in Fig. 7(C). The large-scale flow separation on the airfoil upper surface resulted in the formation of a very large recirculation bubble in the wake the airfoil. As a result, the size of the wake region (i.e., the region with velocity deficit) downstream the airfoil was found to dramatically increase, which indicates a significant increase of the aerodynamic drag force acting on the airfoil, again quantitatively confirmed for the measured drag coefficient data given in Fig. 12.

Although the PIV measurement results given in Fig. 7 clearly reveal the global features of the flow structures around the airfoil,

further details about the transient behavior of the laminar flow separation and evolution of the separation bubble formed on the low-Reynolds-number airfoil cannot be clearly seen due to the limited spatial resolution of the PIV measurements. In order to provide further insights to elucidate underlying physics associated with the laminar flow separation process on low-Reynolds-number airfoils, refined PIV measurements near the nose of the airfoil with much higher spatial resolution ($\Delta/C \approx 0.0045$) were made. The measurement results are shown in Figs. 8, 9, and 11 with the AOA being 6.0 deg, 10.0 deg, and 12.0 deg, respectively.

The laminar boundary layer around the airfoil was clearly visualized as a thin vortex layer affixing to the airfoil upper surface in the typical instantaneous velocity field and the corresponding vorticity distribution shown in Fig. 8. The laminar boundary layer was found to be firmly attached to the airfoil surface when the adverse pressure gradient over the airfoil upper surface is rather mild at relatively small AOA (i.e., AOA < 8.0 deg). The ensemble-averaged velocity field and the streamlines of the mean flow also confirmed that the incoming fluid streams would smoothly flow to follow the streamlined profile of the airfoil when the AOA is relatively small.

As indicated by the surface pressure measurement results described above, a laminar separation bubble would be generated on the airfoil when the AOA became relatively high (i.e., AOA \approx 8.0–12.0 deg). The typical instantaneous velocity field and the corresponding vorticity distribution given in Fig. 9 clearly show that the laminar boundary layer (i.e., the thin vortex layer over the airfoil upper surface) would be “taking off” from the airfoil upper surface at first, and then “landing” on the airfoil upper surface again further downstream. The separation of the laminar boundary layer from the airfoil upper surface and the reattachment of the separated boundary layer can be much more clearly seen from the ensemble-averaged velocity field and the corresponding mean

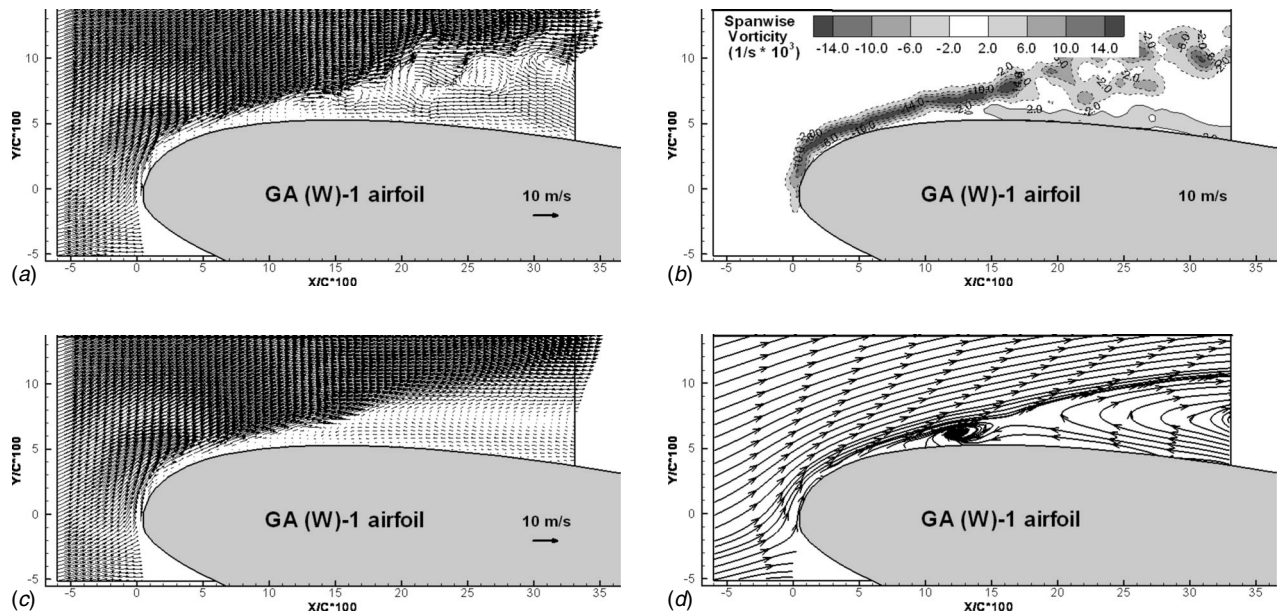


Fig. 11 PIV measurements near the airfoil leading edge with AOA=12.0 deg; (a) instantaneous velocity vectors; (b) instantaneous vorticity distribution; (c) ensemble-averaged velocity vectors; and (d) streamlines of the mean flow

flow streamlines. Based on the PIV measurement results shown in Fig. 9, the location of the separation point (i.e., from where the laminar boundary layer begins to separate from the airfoil surface) was found to be in the neighborhood of $X/C \approx 0.08$, which agrees with the starting point of the “pressure plateau” of the measured surface pressure distribution at 10.0 deg AOA. The reattachment point (i.e., at where the separated boundary layer reattaches to the airfoil surface) was found to be in the neighborhood of $X/C \approx 0.28$, which also agrees well with the estimated location of the reattachment point based on the surface pressure measurements. The laminar separation bubble, which sits in the region between the separation point and the reattachment point, is clearly visualized from the PIV measurement results. While the length of the separation bubble is about 20% of the chord length, the height of the laminar separation bubble is found to be only about 1% of the chord length.

In order to provide further insight into the fundamental physics associated with the turbulent transition and reattachment of the separated laminar boundary layer, PIV measurements with super-fine spatial resolution ($\Delta/C \approx 0.0018$) were made at the rear portion of the laminar separation bubble. The measurement results are shown in Fig. 10 with the airfoil AOA being 10.0 deg.

The PIV measurement results given in Fig. 9 clearly show that the laminar boundary layer would separate from the airfoil upper surface at $X/C \approx 0.08$ due to the severe adverse pressure gradient at 10.0 deg AOA. The instantaneous velocity field and corresponding vorticity distribution given in Fig. 10 reveal that the separated laminar boundary layer behaved more like a free shear layer after separation, which is highly unstable; therefore, rolling up of unsteady vortex structures due to the Kelvin–Helmholtz instabilities and transition to turbulent flow would be readily realized. After the separated laminar boundary layer transits to turbulent flow, the increased entrainment of the turbulent flow made the separated boundary layer reattach to the airfoil upper surface as a turbulent boundary layer, which consequently resulted in the formation of a laminar separation bubble on the airfoil. The reattachment of the separated boundary layer to the airfoil upper surface and consequent formation of the laminar separation bubble can be more clearly seen from the ensemble-averaged velocity field and the streamlines of the mean flow shown in Figs. 10(c) and 10(d).

Figure 10(e) shows the distribution of the measured normalized

Reynolds stress ($-\overline{u'v'}/U_\infty^2$) near the rear portion of the laminar separation bubble. It can be clearly seen that the transition process of the laminar boundary layer is accompanied by the significant increase of Reynolds stress in the flow field. It should be noted that only the contour lines of the normalized Reynolds stress above a critical value of 0.001 are shown in the Fig. 10(e). This critical value has been chosen in the literature to locate the onset of the turbulent transition in separated shear layers [10,17,19]. Following the work of Ol et al. [17], the transition onset position was estimated as the streamwise location where the normalized Reynolds stress first reaches a value of 0.001. The transition onset position at 10.0 deg AOA was found to be located in the neighborhood of $X/C \approx 0.21$ based on the measured Reynolds stress distribution shown in Fig. 10(e). The estimated location was found to agree well with the estimation of the transition point given in Fig. 5, which is based on the surface pressure measurements.

The measured turbulent kinetic energy ($\text{TKE} = 0.5 * (\overline{u'^2} + \overline{v'^2})/U_\infty^2$) distribution at the rear part of the laminar separation bubble is given in Fig. 10(f). It can be clearly seen that the regions with higher TKE was found to be confined in a thin layer in the upstream of the transition point due to the laminar nature of the separated laminar boundary layer. The contour lines of the regions with higher TKE were found to rapidly diverge after the separated laminar boundary layer began to transit to turbulence (i.e., downstream of the transition point). The measured TKE distribution also shows that the regions with higher TKE can be quite close to the airfoil surface wall downstream of the reattachment point (i.e., downstream of location $X/C \approx 0.28$). This confirms that the reattached turbulent boundary layer can entrain more high-speed fluid from outside to the near wall region to make the near wall flow much more energetic compared to the laminar boundary layer upstream of the laminar separation bubble. Therefore, the turbulent boundary layer is much more capable of advancing against an adverse pressure gradient without flow separation. As a result, the reattached turbulent boundary layer can stay attached to the airfoil surface from the reattachment point to the trailing edge of the airfoil, which was confirmed in the PIV measurement results given above.

As the AOA increases to 12.0 deg and higher, the adverse pressure gradient over the upper surface of the airfoil becomes much more significant, and the separation bubble was found to eventu-

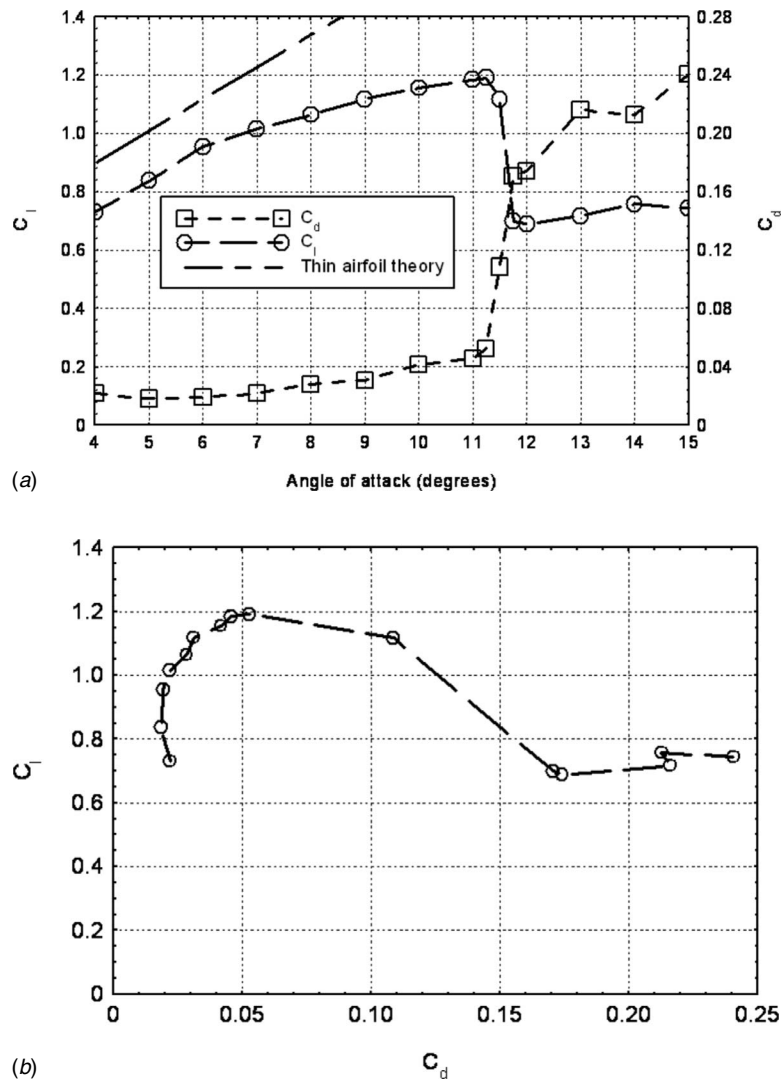


Fig. 12 The measured airfoil lift and drag coefficients; (a) airfoil lift and drag coefficients vs. angle of attack; and (b) lift-drag polar dot

ally burst. As clearly revealed in the instantaneous PIV measurement results given in Fig. 11, the laminar boundary layer was found to separate from the upper surface of the airfoil very near to the airfoil leading edge due to the significant adverse pressure gradient. Although the separated laminar boundary layer was still found to rapidly transit to turbulence by rolling up unsteady vortex structures due to the Kelvin–Helmholtz instabilities, the separated boundary layer could not reattach to the airfoil upper surface anymore due to the much more significant adverse pressure gradient when the AOA became 12 deg and higher. Large-scale flow separation was found to take place over almost entire airfoil upper surface, and the airfoil completely stalled. The airfoil stall is clearly visualized from the PIV measurement results.

3.3 Lift and Drag Coefficients of the Airfoil. The lift and drag coefficients of the airfoil at various AOA were determined by numerically integrating the measured surface pressure distribution around the 2D airfoil model used in the present study. Figure 12 shows the profiles of the measured lift and drag coefficients as the functions of the AOA and a lift-drag polar plot. For reference, the predicted increase rate of the airfoil lift coefficient (i.e., $dC_l/d\alpha = 2\pi$) based on thin airfoil theory [26] is also shown in the figure.

As revealed from the measured surface pressure distributions and PIV measurement results discussed above, the laminar boundary layer was found to firmly attach to the airfoil surface all the

way from the airfoil leading edge to the trailing edge when the adverse pressure gradient over the upper surface of the airfoil is rather mild at relatively small AOA (i.e., $AOA \leq 6.0$ deg). Therefore, the airfoil drag coefficient of the airfoil was found to be very small. The airfoil lift coefficient of the airfoil was found to increase almost linearly with the increasing AOA. The increase rate of the airfoil lift coefficient was found to be almost the same as the prediction based on thin airfoil theory (i.e., $dC_l/d\alpha = 2\pi$) at relatively small AOA when no laminar separation bubble was formed on the airfoil.

The adverse pressure gradient on the airfoil upper surface becomes more and more severe as the AOA increases. Since the laminar boundary layer on the airfoil is unable to withstand the severe adverse pressure gradient [2,3], it will separate from the airfoil upper surface, and laminar flow separation occurs as the AOA relatively becomes large (i.e., $AOA \geq 8$ deg for the present study). The laminar flow separation is evident as the pressure plateau in the measured surface pressure distributions and clearly visualized in the PIV measurement results given above. The separated laminar boundary layer was found to be able to reattach to the upper surface of the airfoil as a turbulent boundary layer after turbulence transition at adequate AOA (i.e., $8.0 \text{ deg} \leq AOA < 12.0$ deg). This results in the formation of a laminar separation bubble on the airfoil upper surface. The airfoil lift coefficient was

found to keep on increasing with the AOA. However, the increase rate of the airfoil lift coefficient was found to considerably degrade due to the formation of a laminar separation bubble. The drag coefficient of the airfoil was found to increase faster with the increasing AOA when the laminar separation bubble was formed on the airfoil. The adverse gradient over the airfoil upper surface became so significant at $AOA \geq 12.0$ deg that the laminar separation bubble was found to burst. The separated laminar boundary layer was not able to reattach to the airfoil upper surface anymore. As visualized in the PIV measurements given above, large-scale flow separation was found to take place over almost the entire airfoil upper surface, and the airfoil was found to completely stall. As a result, the lift coefficient of the airfoil was found to dramatically drop and the drag coefficient was found to significantly increase with the increasing AOA.

4 Conclusion

An experimental investigation was carried out to study the transient behavior of the laminar flow separation on a NASA low-speed GA (W)-1 airfoil at the chord Reynolds number of $Re_C = 70,000$. In addition to conducting surface pressure distribution mapping around the airfoil, a high-resolution PIV system was used to make detailed flow field measurements to quantify the occurrence and behavior of laminar boundary layer separation, transition, and reattachment at various AOA. The detailed flow field measurements were correlated with the surface pressure measurements to elucidate the underlying physics associated with the separation, transition, and reattachment processes of the laminar boundary layer on the low-Reynolds-number airfoil.

The surface pressure mapping and detailed PIV measurements clearly revealed that the laminar boundary layer would stay firmly attached to the airfoil surface as the adverse pressure gradient over the airfoil upper surface was rather mild at relatively small AOA (i.e., $AOA < 8.0$ deg). As the AOA became greater than 8.0 deg, the increased adverse pressure gradient caused the laminar boundary layer to separate from the airfoil upper surface. The separated laminar boundary layer was found to rapidly transit to turbulent flow by generating unsteady Kelvin–Helmholtz vortex structures. When the adverse pressure gradient was adequate (i.e., $AOA < 12.0$ deg), the separated laminar boundary layer was found to be able to reattach to the upper surface of the airfoil as a turbulent boundary layer. As a result, a laminar separation bubble was formed on the airfoil. The length of the laminar separation bubble was found to be about 20% of the airfoil chord length and its height only about 1% of the chord length. While the total length of the laminar separation bubble was found to be almost unchanged regardless the AOA, the length of the laminar portion of the separation bubble was found to slightly increase, and the turbulent portion became slightly shorter with the increasing AOA. The separation bubble was found to move upstream to approach airfoil leading edge as the AOA increased. The laminar separation bubble was found to burst, causing airfoil stall, when the adverse pressure gradient became very significant at $AOA \geq 12.0$ deg.

The detailed PIV measurements elucidated many details about the transient behavior of the laminar boundary layer separation, transition, and reattachment on the low-Reynolds-number airfoil. The transition process of the separated laminar boundary layer was found to be accompanied by the significant increase of Reynolds stress in the flow field. The measured TKE distributions clearly revealed that the reattached turbulent boundary layer was much more energetic, thus more capable of advancing against an adverse pressure gradient without flow separation, compared to the laminar boundary layer upstream the separation bubble. As a result, the reattached turbulent boundary layer was found to stay firmly attached to the airfoil surface from the reattachment point to the trailing edge of the airfoil. The critic points (i.e., separation, transition, and reattachment points) of the separation bubble identified from the PIV measurements were found to agree well with those estimated based on the surface pressure measurements.

The lift coefficient of the airfoil was found to linearly increase with the increasing AOA when the AOA is relatively small, while the drag coefficient of the airfoil was found to be very small. After the formation of the laminar separation bubble on the airfoil at $AOA \geq 8.0$ deg, the increase rate of the airfoil lift coefficient was found to considerably degrade and the airfoil drag coefficient was found to increase much faster with increasing AOA. As the AOA became much higher (i.e., $AOA \geq 12.0$ deg), where the separation bubble was found to burst to cause airfoil stall, the lift coefficient of the airfoil was found to dramatically drop, and the airfoil drag coefficient was found to significantly increase.

Acknowledgment

The authors want to thank Mr. Bill Rickard, Mr. De Huang, and Mr. Masatoshi Tamai of Iowa State University for their help in conducting the experiments. The support of National Science Foundation CAREER program under Award No. CTS-0545918 is gratefully acknowledged.

References

- [1] Tani, I., 1964, "Low Speed Flows Involving Bubble Separations," *Prog. Aeronaut. Sci.*, Vol. 5, pp. 70–103.
- [2] Carmichael, B. H., 1981, "Low Reynolds Number Airfoil Survey," NASA CR-165803, Vol. 1.
- [3] Lissaman, P. B. S., 1983, "Low-Reynolds-Number Airfoils," *Annu. Rev. Fluid Mech.*, 15, pp. 223–239.
- [4] J. T. Mueller, ed., 2001, *Fixed and Flapping Wing Aerodynamics for Micro Air Vehicle Applications*, Progress in Astronautics and Aeronautics, Vol. 195, AIAA.
- [5] Gad-el-Hak, M., 2001, "Micro-Air-Vehicles: Can They be Controlled Better," *J. Aircr.*, 38(3), pp. 419–429.
- [6] Horton, H. P., 1968, Laminar Separation in Two and Three-Dimensional Incompressible Flow, Ph.D. thesis, University of London.
- [7] Hatman, A., and Wang, T., 1999, "A Prediction Model for Separated Flow Transition," *ASME J. Turbomach.*, 121, pp. 594–602.
- [8] Johnson, M. W., 1994, "A Bypass Transition Model for Boundary Layers," *ASME J. Turbomach.*, 116, pp. 759–764.
- [9] Solomon, W. J., Walker, G. J., and Gostelow, J. P., 1996, "Transition Length Prediction for Flows With Rapidly Changing Pressure Gradients," *ASME J. Turbomach.*, 118, pp. 744–751.
- [10] Volino, R. J., and Hultgren, L. S., 2001, "Measurements in Separated and Transitional Boundary Layers Under Low-Pressure Turbine Airfoil Conditions," *ASME J. Turbomach.*, 123, pp. 189–197.
- [11] Haeuelsen, V., Henneke, D. K., and Schröder, T., 1997, "Measurements With Surface Mounted Hot Film Sensors on Boundary Layer Transition in Wake Disturbed Flow," AGARD CP-598.
- [12] Zhong, S., Kittichaikarn, C., Hodson, H. P., and Ireland, P. T., 2000, "Visualization of Turbulent Spots Under the Influence of Adverse Pressure Gradients," *Exp. Fluids*, 28, pp. 385–393.
- [13] Fitzgerald, E. J., and Mueller, T. J., 1990, "Measurements in a Separation Bubble on an Airfoil Using Laser Velocimetry," *AIAA J.*, 28(4), pp. 584–592.
- [14] Brendel, M., and Mueller, T. J., 1987, "Boundary Layer Measurements on an Airfoil at Low Reynolds Numbers," AIAA Paper No. 87-0495.
- [15] O'Meara, M. M., and Mueller, T. J., 1987, "Laminar Separation Bubble Characteristics on an Airfoil at Low Reynolds Numbers," *AIAA J.*, 25(8), pp. 1033–1041.
- [16] Lang, M., Rist, U., and Wagner, S., 2004, "Investigations on Controlled Transition Development in a Laminar Separation Bubble by Means of LDA and PIV," *Exp. Fluids*, 36, pp. 43–52.
- [17] Ol, M. V., Hanff, E., McAuliffe, B., Scholz, U., and Kaehler, C., 2005, "Comparison of Laminar Separation Bubble Measurements on a Low Reynolds Number Airfoil in Three Facilities," *35th AIAA Fluid Dynamics Conference and Exhibit*, Toronto, Ontario, June 6–9, AIAA Paper 2005-5149.
- [18] Raffel, M., Favier, D., Berton, E., Rondot, C., Nsimba, M., and Geissler, M., 2006 "Micro-PIV and ELDV Wind Tunnel Investigations of the Laminar Separation Bubble Above a Helicopter Blade Tip," *Meas. Sci. Technol.*, 17, pp. 1652–1658.
- [19] Burgmann, S., Brücker, S., Schröder, W., 2006, "Scanning PIV Measurements of a Laminar Separation Bubble," *Exp. Fluids*, 41, pp. 319–326.
- [20] Gao, H., Hu, H., and Wang, Z. J., 2008, "Computational Study of Unsteady Flows Around Dragonfly and Smooth Airfoils at Low Reynolds Numbers," *46th AIAA Aerospace Sciences Meeting and Exhibit*, Reno, NV, Jan. 7–10, AIAA Paper No. 2008-0385.

- [21] McGee, R. J., and Beasley, W. D., 1973, "Low-Speed Aerodynamics Characteristics of a 17-Percent-Thick Airfoil Section Designed for General Aviation Applications," NASA TN D-7428.
- [22] Russell, J., 1979, "Length and Bursting of Separation Bubbles: A Physical Interpretation," Science and Technology of Low Speed Motorless Flight, NASA Conference Publication 2085, Part 1.
- [23] Shum, Y. K., and Marsden, D. J., 1994, "Separation Bubble Model for Low Reynolds Number Airfoil Applications," *J. Aircr.*, **31**(4), pp. 761–766.
- [24] Yaruseych, S., Sullivan, P. E., and Kawall, J. G., 2006, "Coherent Structure in an Airfoil Boundary Layer and Wake at Low Reynolds Numbers," *Phys. Fluids*, **18**, 044101.
- [25] Lin, J. C. M., and Pulley, L. L., 1996, "Low-Reynolds-Number Separation on an Airfoil," *AIAA J.*, **34**(8), pp. 1570–1577.
- [26] Anderson, J. D., 2005, *Fundamentals of Aerodynamics*, 4th ed., McGraw-Hill Higher Education, New York.